Applied Energy 87 (2010) 2666–2672

Contents lists available at ScienceDirect

Applied Energy

journal homepage: www.elsevier.com/locate/apenergy

Thermal characteristics of shape-stabilized phase change material wallboard with periodical outside temperature waves

Guobing Zhou [a], Yongping Yang [a,*], Xin Wang [b], Jinming Cheng [a]

[a] School of Energy and Power Engineering, School of Renewable Energy, Beijing Key Laboratory of Security and Clean Energy Technology, North China Electric Power University, Beijing 102206, PR China
[b] Department of Building Science, School of Architecture, Tsinghua University, Beijing 100084, PR China

ARTICLE INFO

Article history:
Received 21 June 2009
Received in revised form 27 November 2009
Accepted 1 February 2010
Available online 2 March 2010

Keywords:
Energy storage
Shape-stabilized phase change material
Thermal characteristics
Decrement factor

ABSTRACT

Thermal characteristics of shape-stabilized phase change material (SSPCM) wallboard with sinusoidal temperature wave on the outer surface were investigated numerically and compared with traditional building materials such as brick, foam concrete and expanded polystyrene (EPS). One-dimensional enthalpy equation under convective boundary conditions was solved using fully implicit finite-difference scheme. The simulation results showed that the SSPCM wallboard presents distinct characteristics from other ordinary building materials. Phase transition keeping time of inner surface and decrement factor were applied to analyze the effects of PCM thermophysical properties (melting temperature, heat of fusion, phase transition zone and thermal conductivity), inner surface convective heat transfer coefficient and thickness of SSPCM wallboard. It was found that melting temperature is one important factor which influences both the phase transition keeping time and the decrement factor; for a certain outside temperature wave, there exist critical values of latent heat of fusion and thickness of SSPCM above which the phase transition keeping time or the decrement factor are scarcely influenced; thermal conductivity of PCM and inner surface convective coefficient have little effect on the phase transition keeping time but significantly influence the decrement factor; and the phase transition zone leads to small fluctuations of the original flat segment of inner surface temperature line. The results aim to be useful for the selection of SSPCMs and their applications in passive solar buildings.

1. Introduction

Energy consumption of a building and indoor comfort are related to the outdoor climate condition, the building construction and materials, the indoor heat disturbance and ventilation, etc. For a building located in a specific region with given indoor heat source and air change per hour (ACH), the thermal performance of the building is strongly influenced by the thermophysical properties of the construction materials [1,2]. For instance, as Asan and Sancaktar [3] and Ulgen [4] have pointed out, large heat capacity of a wall material results in high "time lags" and reduces room temperature swings due to the effect of thermal storage. However, traditional building materials such as brick and concrete store heat in sensible form and then large structural mass is usually required.

Large quantity of thermal storage/recovery can be achieved in the form of latent heat by melting/freezing a phase change material (PCM). And little or no change in temperature occurs during this phase transition process. Therefore, PCM can be incorporated into wall materials to enhance thermal energy storage capacities of buildings particularly for passive solar applications, peak load shifting, etc. Peippo et al. [5] analyzed the effect of using PCM (fatty acid) walls in a direct-gain passive solar house and direct energy savings of 5–20% were expected. Experimental and simulation studies by Athienitis et al. [6] showed that utilization of the PCM gypsum board as inside wall linings in a full-scale outdoor test room may reduce the maximum room temperature by about 4 °C during the day and can reduce the heating load at night significantly. Neeper [7] examined the thermal dynamics of gypsum wallboards impregnated by fatty acids and paraffin waxes as PCM which were subjected to the diurnal variation of room temperature. He found that the diurnal storage achieved in practice may be limited to the range 300–400 kJ m^{-2}, even if the wallboard has a greater latent capacity. Numerical results by Heim and Clarke [8] also showed that the solar energy stored in the PCM gypsum panels can reduce heating energy demand by up to 90% during the heating season. Most of the above PCM composites are prepared by immersing wallboard into PCM or by direct incorporation at the mixing stage of wallboard production. The disadvantage of these two methods is the leakage which may be a problem over a long period of time, and this also limits the amount of PCM

* Corresponding author. Tel.: +86 10 61772713; fax: +86 10 51963903.
E-mail address: yyp@ncepu.edu.cn (Y. Yang).

0306-2619/$ - see front matter © 2010 Elsevier Ltd. All rights reserved.
doi:10.1016/j.apenergy.2010.02.001

Nomenclature

a	coefficient in discretized equation
A	amplitude of temperature wave
ACH	air change per hour
c_p	specific heat (J kg^{-1} °C^{-1})
dt	phase transition zone (°C)
f	decrement factor
h	convective heat transfer coefficient (W m^{-2} °C^{-1})
H	enthalpy (kJ kg^{-1})
k	thermal conductivity (W m^{-1} °C^{-1})
L	thickness (mm)
SSPCM	shape-stabilized phase change material
t	temperature (°C)
x	position along the direction of the board thickness (mm)

Greek letters

ρ	density (kg m^{-3})
τ	time (s)
φ	time lag (h)
ψ	phase transition keeping time (h)
ε	convergence precision
ω	relaxation factor
Δ	step difference

Subscripts

a	air
in	inside
$init$	initial
j	space grid node
l	liquid state of PCM
m	phase transition state of PCM
M1	node at the right boundary face
n	temporal node
out	outside
p	PCM
s	solid state of PCM
w	wallboard

(usually 20–30%) in the wallboard. In most recent years, Inaba and Tu [9], Xiao et al. [10] and Zhang et al. [11] investigated a kind of novel compound PCM, the so-called shape-stabilized PCM (SSPCM) for latent thermal storage. It consists of paraffin as dispersed PCM and high density polyethylene (HDPE) or other materials as supporting material. Since the mass percentage of paraffin can be as much as 80% or so, the total stored energy is comparable with that of traditional PCMs. As Ye and Ge [12] have pointed out, the other advantage of this kind of PCM is that as long as the operating temperature is below the melting point of the supporting material, the compound material can keep its shape even when the PCM changes from solid to liquid. This reduces the liquid PCM leakage danger and it can be used for thermal storage in buildings without encapsulation.

To maximize the benefit from the heat storage, thermal characteristics of building materials need to be clarified. In the researches by Asan and Sancaktar [3] and Ulgen [4], "time lag" φ and "decrement factor" f were applied to analyze the effect of common building materials under periodic convection boundary conditions. φ and f respectively describe the time and amplitude variations for heat waves propagating from outside to the inner surface of the wall. For those traditional building materials, thermophysical properties vary slightly with temperature and the heat wave propagation could be regarded as a linear process. Therefore, the variation of the inner surface temperature is similar to that of the outdoor temperature. While for PCMs which undergo phase transition from solid to liquid or vice versa, the equivalent specific heat capacity changes significantly with temperature. This leads to the nonlinear characteristics of heat transfer equations and then the heat wave propagation tends to be nonlinear consequently. Zhang et al. [13] put forward two new parameters, i.e. modifying factor of the inner surface heat flux 'a' and the ratio of the thermal storage 'b', to analyze the thermal storage of PCM wallboard.

For the sake of selection of SSPCMs and their applications and design in passive solar buildings, thermal characteristics of SSPCM board need to be clear. Therefore, the aim of the present work is to discuss the inner surface temperature variation of a SSPCM wallboard which is subjected to periodic outdoor temperature waves and compare it with that of traditional building materials – brick, foam concrete and expanded polystyrene (EPS). Effects of several factors on the SSPCM wallboard characteristics are then discussed.

2. Analysis method

The problem now investigated is a SSPCM wallboard shown in Fig. 1. On both sides of the SSPCM wallboard, convection boundary conditions are present. To the outside of the SSPCM, the 'sol–air temperature' is assumed to show sinusoidal variations from 10 °C to 25 °C during a day period. As Asan and Sancaktar [3] have pointed out, this sol–air temperature includes the effect of solar radiation combined with outside air temperature. While at the inner side of the SSPCM wallboard, the air temperature is kept constant at 20 °C. The present work aims to make a numerical analysis on the inner surface temperature variations of the SSPCM wallboard. Calculations are also carried out on brick, foam concrete and expanded polystyrene (EPS) wallboards for comparison with SSPCM. These three materials respectively represent the heavyweight, lightweight and insulation materials commonly used in building envelopes. Furthermore, for SSPCM, effecting factors such as PCM thermophysical properties (melting temperature, heat of fusion, phase transition zone and thermal conductivity), inner surface convective heat transfer coefficient, and thickness of SSPCM wallboard are analyzed.

An enthalpy model [14] is applied for this simulation, in which enthalpy is used as the primary variable and temperature is calculated from enthalpy by the correlation between them. This method simplifies the solution of the problem without explicit tracking of the solid–liquid interface. It is assumed that heat transfer through the PCM board is one dimensional and time dependent. The governing equation is written as:

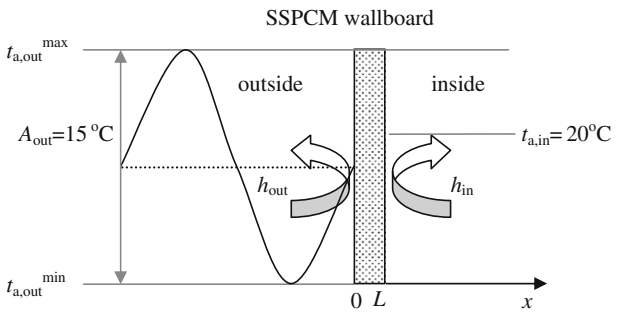

Fig. 1. Schematic sketch of the convection heat transfer condition of the SSPCM wallboard.

$$\rho\frac{\partial H}{\partial \tau}=k\frac{\partial^2 t}{\partial x^2}\ 0\leqslant x\leqslant L \tag{1}$$

where the enthalpy of PCM is the function of temperature described as:

$$H=\begin{cases}\int_{t_0}^{t} c_{p,s}dtt<t_1\\ \int_{t_0}^{t_1} c_{p,s}dt+\int_{t_1}^{t} c_{p,m}dtt_1\leqslant t\leqslant t_2\\ \int_{t_0}^{t_1} c_{p,s}dt+\int_{t_1}^{t_2} c_{p,m}dt+\int_{t_2}^{t} c_{p,l}dtt>t_2\end{cases} \tag{2}$$

Here, t_0 is the temperature point where the enthalpy is zero and the phase transition occurs within a small temperature range from t_1 to t_2. The equivalent specific heat capacity during the phase transition process for SSPCM is also assumed to be uniform, i.e. $c_{p,m}=H_m/(t_2-t_1)$. Research by Li et al. [15] showed that little calculation error has been caused by this simplification. $c_{p,s}$ and $c_{p,l}$ are the constant specific heat capacities in the solid and liquid states, respectively. For constant-thermophysical-property materials, $H=\int_{t_0}^{t} c_{p,s}dt$.

The initial condition is:

$$t(x,\tau)|_{\tau=0}=t_{init} \tag{3}$$

For surfaces exposed to the outside and inside air, the boundary conditions are:

$$h_{out}(t_{out}-t_{p,out})=-k_p\left.\frac{\partial t}{\partial x}\right|_{x=0} \tag{4}$$

$$h_{in}(t_{in}-t_{p,in})=k_p\left.\frac{\partial t}{\partial x}\right|_{x=L} \tag{5}$$

h_{out} and h_{in} are the outside and inside convective heat transfer coefficients, respectively.

3. Numerical solution

The aforementioned equations are solved numerically using a control volume-based fully implicit finite-difference scheme. Along the direction of thickness, the computational domain of wallboard is discretized uniformly. Fig. 2 shows the generated spatial and temporal grid nodes.

Then, Eq. (1) is discretized using central difference in space and backward Euler method in time to ensure the convergence and stability of numerical solution. The resultant discretized equation for inside nodes takes the following form:

$$H_j^{n+1}=H_j^n+a_{j+1}t_{j+1}^{n+1}+a_{j-1}t_{j-1}^{n+1}-a_jt_j^{n+1}\ (3\leqslant j\leqslant \mathrm{M1}-2) \tag{6}$$

where

$$a_{j+1}=\frac{\Delta\tau\cdot k_{j+1/2}^{n+1}}{\rho(\Delta x)^2}=\frac{\Delta\tau\cdot 2k_j^{n+1}k_{j+1}^{n+1}}{\rho(\Delta x)^2(k_j^{n+1}+k_{j+1}^{n+1})} \tag{7}$$

$$a_{j-1}=\frac{\Delta\tau\cdot k_{j-1/2}^{n+1}}{\rho(\Delta x)^2}=\frac{\Delta\tau\cdot 2k_{j-1}^{n+1}k_j^{n+1}}{\rho(\Delta x)^2(k_{j-1}^{n+1}+k_j^{n+1})} \tag{8}$$

$$a_j=a_{j-1}+a_{j+1} \tag{9}$$

As shown in Eqs. (7) and (8), the thermal conductivity at each interface is calculated using harmonic mean value of the two nodes at the left and right sides of the interface, respectively.

Temperatures of the boundary nodes "1" and "M1" are determined according to the energy balance at the surfaces, which are:

$$t_1^{n+1}=\left(t_{out}^{n+1}+\frac{k_1^{n+1}}{h_{out}\Delta x/2}t_2^{n+1}\right)\Big/\left(1+\frac{k_1^{n+1}}{h_{out}\Delta x/2}\right) \tag{10}$$

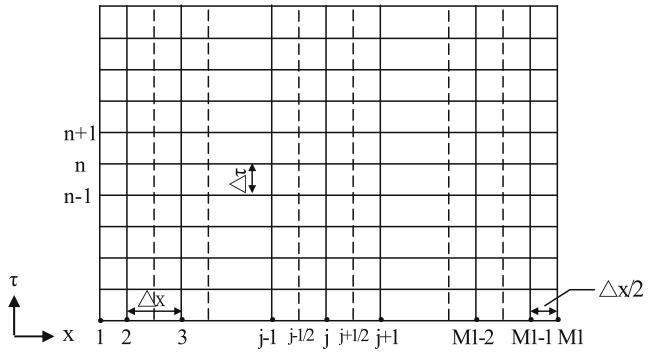

Fig. 2. Sketch of the generated grids.

$$t_{\mathrm{M1}}^{n+1}=\left(t_{in}^{n+1}+\frac{k_{\mathrm{M1}}^{n+1}}{h_{in}\Delta x/2}t_{\mathrm{M1}-1}^{n+1}\right)\Big/\left(1+\frac{k_{\mathrm{M1}}^{n+1}}{h_{in}\Delta x/2}\right) \tag{11}$$

For the two nodes neighboring to the boundary surfaces, i.e. "2" and "M1-1", the additional source term method [16] is used and the discretized equations can take the following form without including the boundary nodes:

$$H_2^{n+1}=H_2^n+\frac{\Delta\tau}{\rho(\Delta x)^2}\left[\frac{2k_3^{n+1}k_2^{n+1}}{k_3^{n+1}+k_2^{n+1}}t_3^{n+1}-\left(\frac{2k_3^{n+1}k_2^{n+1}}{\left(k_3^{n+1}+k_2^{n+1}\right)}+\frac{1}{1/(h_{out}\Delta x)+1/\left(2k_1^{n+1}\right)}\right)t_2^{n+1}+\frac{t_{out}^{n+1}}{1/(h_{out}\Delta x)+1/\left(2k_1^{n+1}\right)}\right] \tag{12}$$

$$H_{\mathrm{M1}-1}^{n+1}=H_{\mathrm{M1}-1}^n+\frac{\Delta\tau}{\rho(\Delta x)^2}\left[\frac{2k_{\mathrm{M1}-2}^{n+1}k_{\mathrm{M1}-1}^{n+1}}{k_{\mathrm{M1}-2}^{n+1}+k_{\mathrm{M1}-1}^{n+1}}t_{\mathrm{M1}-2}^{n+1}-\left(\frac{2k_{\mathrm{M1}-2}^{n+1}k_{\mathrm{M1}-1}^{n+1}}{k_{\mathrm{M1}-2}^{n+1}+k_{\mathrm{M1}-1}^{n+1}}+\frac{1}{1/(h_{in}\Delta x)+1/\left(2k_{\mathrm{M1}}^{n+1}\right)}\right)t_{\mathrm{M1}-1}^{n+1}+\frac{t_{in}}{1/(h_{in}\Delta x)+1/\left(2k_{\mathrm{M1}}^{n+1}\right)}\right] \tag{13}$$

Eqs. (6)–(13) represent a system of algebraic equations of the same size as the number of discrete nodes. This system is numerically solved by employing successive over relaxation (SOR) iteration algorithm. The relaxation factor used here is $\omega=1.5$. When the maximum enthalpy difference between two iterations, $\max|\Delta H_j|$, is less than the given precision ($\varepsilon=10^{-5}$ J kg^{-1}), the obtained enthalpy and temperature are recorded and the calculation proceeds to the next time step. Fig. 3 shows the flow chart of the calculation. The space grid size for the PCM board is 0.5 mm and the time step is one minute. Further refinement of either space grids or time steps shows no effect on the calculation results. The calculation proceeds for many cycles to eliminate the effect of the initial conditions.

4. Model validation

The model is verified by comparison with data in literature for cases of both the PCM board [17] and the constant-thermophysical-property material – concrete [18]. For PCM board, Solomon [17] analyzed an N-Eicosene paraffin slab with initial uniform temperature of 21 °C which increased on one side at constant temperature of 95 °C. The temperature distribution of the slab after an hour is examined. Table 1 shows the comparison of the present model simulations with the exact temperature data and Solomon's approximate solutions. It is indicated that the present model agrees quite well with the original data by maximum discrepancy of ±2%.

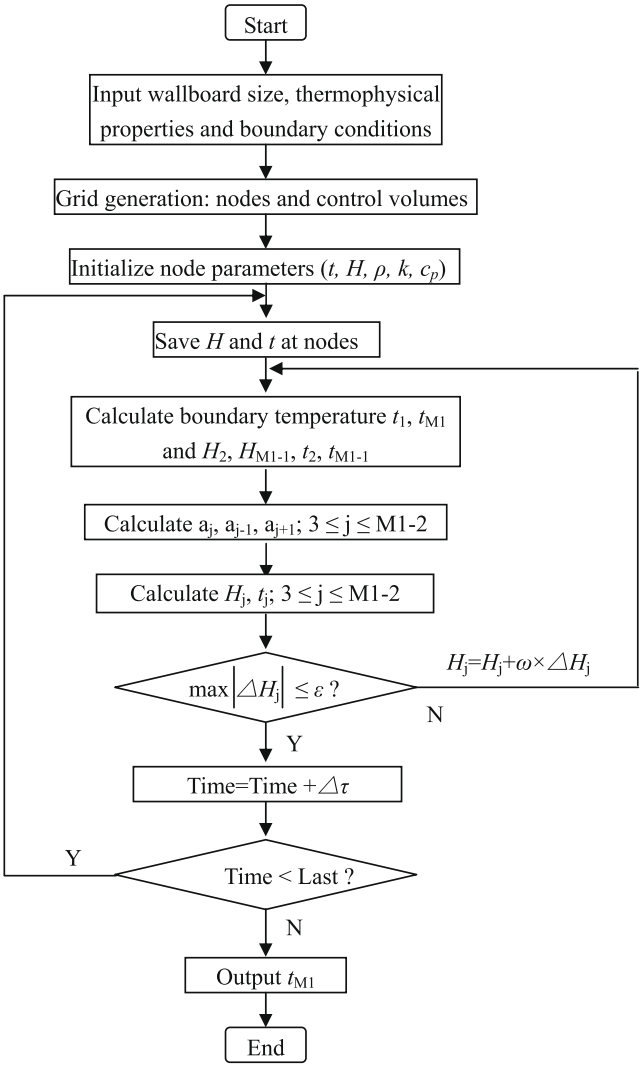

Fig. 3. Flow chart of the numerical solution.

For the case of constant-thermophysical-property material, a concrete wall under periodic outside sol–air temperature wave is used to validate the present model. The inside temperature in this problem is also kept constant and the inner surface temperature is then calculated. Threlkeld [18] gave an analytical solution to this problem. Fig. 4 shows that the present model also agrees well with Threlkeld's analytical results.

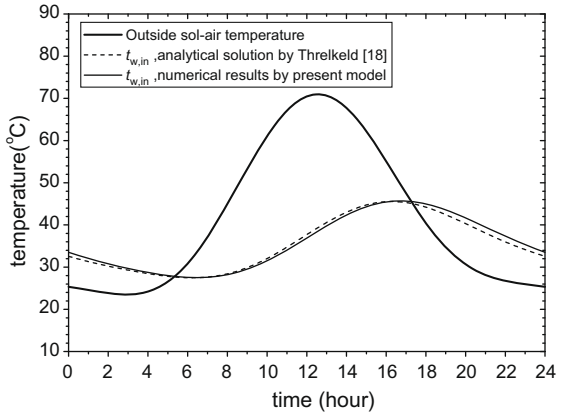

Fig. 4. Comparison of the present computation with analytical solution of Threlkeld [18].

Table 1
Comparison of the present model with the temperature distribution data from Solomon [17] (t_m = 36.7 °C, H_m = 247 kJ kg^{-1}, k = 0.1 5 W m^{-1} °C^{-1}), L = 0.15 m).

X (cm)	Exact temperature data from Solomon [17] (°C)	Approximate solution by Solomon [17] (°C)	Results of the present model (°C)	Deviation of the present model (%)
0	95	95	95	0
0.2	86.78	87.11	88.47	1.95
0.4	78.6	79.22	79.81	1.54
0.6	70.52	71.92	71.26	1.05
0.8	62.58	64.01	62.92	0.54
1	54.83	56.43	54.87	0.07
1.2	47.29	49.16	47.24	-0.11
1.4	40.02	42.23	40.11	0.22
1.6	35.72	36.34	35.92	0.56
1.8	34.18	34.76	34.39	0.61
2	32.73	33.27	32.96	0.70
2.2	31.38	31.88	31.63	0.8
2.4	30.13	30.58	30.41	0.93
2.6	28.99	29.37	29.29	1.03
2.8	27.95	28.26	28.26	1.11
3	27.01	27.25	27.33	1.18
3.2	26.17	26.33	26.49	1.22
3.4	25.42	25.5	25.74	1.26
3.6	24.75	24.77	25.07	1.29
3.8	24.17	24.13	24.47	1.24
4	23.66	23.59	23.95	1.23
4.2	23.21	23.14	23.49	1.21
4.4	22.83	22.79	23.09	1.14
4.6	22.51	22.53	22.75	1.07
4.8	22.23	22.37	22.46	1.03
5	22	21.95	22.21	0.95
5.2	21.81	21.85	22	0.87
5.4	21.65	21.74	21.83	0.83
5.6	21.52	21.63	21.68	0.74
5.8	21.41	21.52	21.57	0.75
6	21.32	21.41	21.48	0.75
6.2	21.25	21.31	21.41	0.75
6.4	21.2	21.2	21.36	0.75
6.6	21.15	21.09	21.33	0.85
6.8	21.12	21.0	21.32	0.95

5. Results and discussion

At first, the variations of inner surface temperature are calculated to compare the thermal characteristics of SSPCM, brick, foam concrete and expanded polystyrene (EPS) wallboards under the same outdoor sinusoidal temperature waves. Table 2 lists the thermophysical properties of these four materials and convective heat transfer coefficients on the wallboard surfaces. For SSPCM, the typical bold figures in the table are used for calculation when com-

Table 2
Thermophysical properties and convective heat transfer coefficients for wallboard materials.

Parameters	SSPCM	Solid brick	Foam concrete	EPS
t_m (°C)	18, **20**, 22	–	–	–
H_m (kJ kg^{-1})	30, 60, 90, **120**, 150	–	–	–
dt (°C)	**0.2**, 1.0, 2.0, 5.0	–	–	–
c_p (J kg^{-1} °C^{-1})	**2000**	**880**	**1000**	**1380**
k (W m^{-1} °C^{-1})	0.1, **0.2**, 0.5, 1.0, 2.0	**0.62**	**0.22**	**0.042**
ρ (kg m^{-3})	**850**	**1800**	**700**	**30**
L (mm)	10, 15, **20**, 30	**20**	**20**	**20**
h_{out} (W m^{-2} °C^{-1})	8.7, **18.6**, 25.4	**18.6**	**18.6**	**18.6**
h_{in} (W m^{-2} °C^{-1})	2.5, 5.4, **8.7**, 15.4	**8.7**	**8.7**	**8.7**

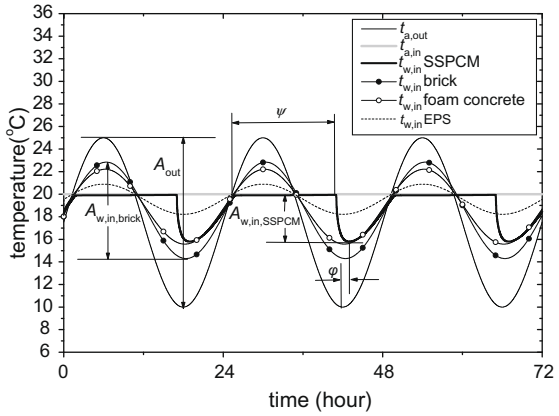

Fig. 5. Comparison of inner surface temperature for SSPCM, brick, foam concrete and EPS.

pared with the other three materials. Fig. 5 shows the simulation results of inner surface temperature variations. It can be seen that for the brick, foam concrete and EPS wallboards, the inner surface temperature lines keep the sinusoidal wave style with only the time lagged and the amplitude decreased. However, there exist flat segments within the inner surface temperature lines of SSPCM wallboard and the wave amplitude is considerably decreased. This is due to the fact that when the sinusoidal temperature wave propagates from the outside to the inner side of the SSPCM wall, the SSPCM is melted or solidified within a narrow temperature range. Therefore, the inner surface temperature will keep constant at or near the melting temperature until the phase transition ends.

Similar to the case for traditional wall materials, '*decrement factor*' (f) is also defined as the ratio of the wallboard inner surface temperature wave amplitude ($A_{w,in}$) to the outdoor temperature wave amplitude (A_{out}), i.e. $f = A_{w,in}/A_{out}$. And the 'time lag' (φ) can also be defined as the time delayed when the temperature wave reaches the low level from the outside to the inner surface of wallboard. For the case in Fig. 5, the SSPCM wallboard gives the largest time lag and the EPS gives the smallest time lag due to the highest thermal diffusivity, i.e. $\varphi_{SSPPCM} = 0.98$ h, $\varphi_{brick} = 0.41$ h, $\varphi_{foam\ concrete} = 0.21$ h, $\varphi_{EPS} = 0.03$ h; While EPS produces the lowest decrement factor and the brick gives the highest decrement factor due to its highest thermal conductivity, i.e. $f_{SSPPCM} = 0.28$, $f_{brick} = 0.57$, $f_{foam\ concrete} = 0.44$, $f_{EPS} = 0.18$. These results confirm the analysis for different building materials by Asan [19].

However, it can also be found that although there is not much difference between the thermal conductivities of SSPCM and foam concrete, the SSPCM gives much lower decrement factor than the foam concrete due to the nearly constant temperature characteristics during the melting/freezing process. As long as the phase transition lasts, the inner surface temperature will keep constant at or near the melting point, which indicates the advantage of using PCM to improve the indoor thermal comfort for a long time. For convenience of analysis, the time that the wallboard inner surface temperature keeps constant at or near the phase transition point is called as '*phase transition keeping time*' or '*flat time*' (ψ in Fig. 5, for one wave length period). ψ and f are the two important characteristics to analyze the thermal behavior of SSPCM wallboard.

The computations are then repeated to investigate the effects of several factors on the SSPCM wallboard thermal characteristics. The effecting factors considered include thermophysical properties such as melting temperature, heat of fusion, phase transition zone and thermal conductivity of the SSPCM as well as inner surface convective heat transfer coefficient and thickness of the SSPCM wallboard. In each parametric analysis, only one specific parameter is changed, whereas the others are kept constant when the simulation is carried out.

Fig. 6 shows the hourly inner surface temperature for various melting temperatures of the SSPCM. It is indicated that for different melting temperature (t_m) of SSPCM, the corresponding ψ and f are also different. For $t_m = 18$ °C, $\psi = 18.7$ h, $f = 0.27$; for $t_m = 20$ °C, $\psi = 15.5$ h, $f = 0.28$; for $t_m = 22$ °C, $\psi = 9.4$ h, $f = 0.33$. This is due to the fact that with the melting temperature rising up, the available heat that could be stored by SSPCM tends to be less and then the shorter charge and discharge time are needed.

Fig. 7 presents the inner surface temperature variation for different heat of fusions (H_m) of SSPCM. It is clear that ψ is relatively small for the cases of small heat of fusion, i.e. $H_m = 30$ kJ kg^{-1} and $H_m = 60$ kJ kg^{-1}. With outdoor temperature rising up in early hours, the inner surface temperature also increases at first and then keeps constant at the melting point, which indicates that the inner surface PCM begins to melt. However, with time proceeding forward, the inner surface temperature, for cases of $H_m = 30$ kJ kg^{-1} and $H_m = 60$ kJ kg^{-1}, begins to rise up again, which means that the PCM has been fully melted to liquid state. After the inner surface temperature reaches some top point, it begins to fall down following the descending outdoor temperature and keeps constant at the melting temperature again due to the fact that the liquid PCM begins to solidify. After the inner surface PCM is fully solidified, i.e. the flat time period ends, the inner surface temperature falls down again till some bottom point due to the consistently descending outdoor temperature.

The above description indicates that there exist fluctuations of inner surface temperature between the two flat time periods for

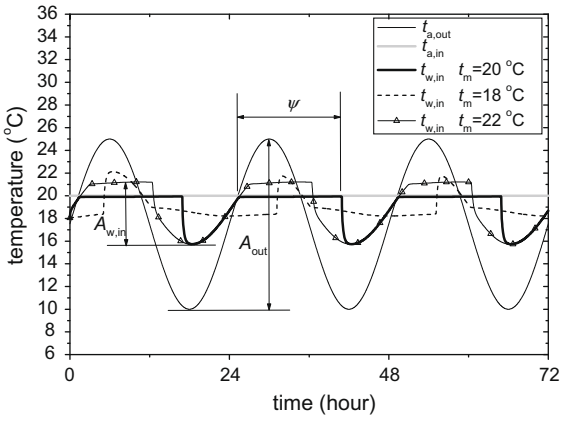

Fig. 6. Hourly inner surface temperature for various melting temperature of the SSPCM.

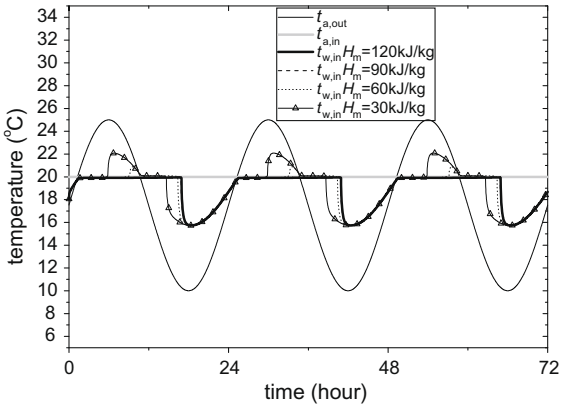

Fig. 7. Hourly inner surface temperature for various heat of fusion of the SSPCM.

cases of H_m = 30 kJ kg^{-1} and H_m = 60 kJ kg^{-1} due to the low values of heat of fusion. While for cases of H_m = 90 kJ kg^{-1} and H_m = 120 kJ kg^{-1} in Fig. 7, the inner surface temperature keeps constant at the phase transition point (i.e. no up-and-down appears) from the beginning of melting process till the end of freezing process due to the high latent heat of fusion. It can also be found that ψ and f are same for cases of both H_m = 90 kJ kg^{-1} and H_m = 120 kJ kg^{-1}. This suggests that, corresponding to some certain outdoor temperature wave, there exists a critical value of heat of fusion for SSPCM beyond which the inner surface temperature is not affected.

Fig. 8 gives the hourly inner surface temperature for various thermal conductivities (k) of SSPCM. It appears that thermal conductivity has no obvious effect on ψ but significantly influences the decrement factor f. This is similar to that of traditional building materials with constant thermophysical properties. For k = 0.1 W m^{-1} °C^{-1}, f = 0.21; k = 0.2 W m^{-1} °C^{-1}, f = 0.29; k = 0.5, f = 0.37; k = 2.0 W m^{-1} °C^{-1}, f = 0.43. It seems that when the conductivity is above 0.5 W m^{-1} °C^{-1}, its influence on the decrement factor tends to be weakened. Most organic PCMs have thermal conductivities as low as 0.2–0.3 W m^{-1} °C^{-1}. Recently, Wang et al. [20,21] added β-Aluminum nitride and expanded graphite into the organic SSPCMs to improve the thermal conductivities by up to 87.8% and 440%, respectively.

Fig. 9 shows the effect of wallboard thickness on the inner surface temperature. It can be seen that there is also an appropriate value of thickness above which ψ does not change and the effect on the decrement factor f tends to be weakened either.

Technical-grade PCMs usually have a phase transition zone rather than a sharp melting point. From Fig. 10, we see that a narrow phase transition zone leads to small fluctuation of the original flat inner surface temperature line.

Fig. 11 shows the hourly variation of inner surface temperature for different convective heat transfer coefficients between the inner surface and the air. Similar to the thermal conductivity, the change of convective heat transfer coefficient has no effect on ψ but significantly influences the decrement factor f. However, the inside convective heat transfer coefficient calculated with natural convective formula in ASHRAE handbook [22] is much low (about 2 W m^{-2} °C^{-1}) which limits the availability of the latent storage and this problem still needs to be addressed. Most recently, Liu and Awbi [23] reported their experimental work on the performance of PCM boards under natural convection and their results showed that the heat transfer coefficient between the PCM wall and indoor air can be up to 4.43 W m^{-2} °C^{-1} due to the increased energy exchange. Similar results were also given by Kuznik and Virgone [24].

Fig. 12 presents the effect of outer surface convective heat transfer coefficient on inner surface temperature. Similarly, the change of outer surface convective heat transfer coefficient only has influences on the decrement factor f. It shows that there is little difference between the decrement factors for h_{out} = 18.6

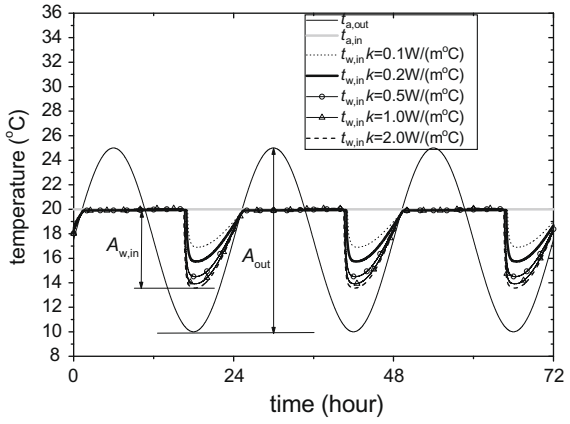

Fig. 8. Hourly inner surface temperature for various thermal conductivity of the SSPCM.

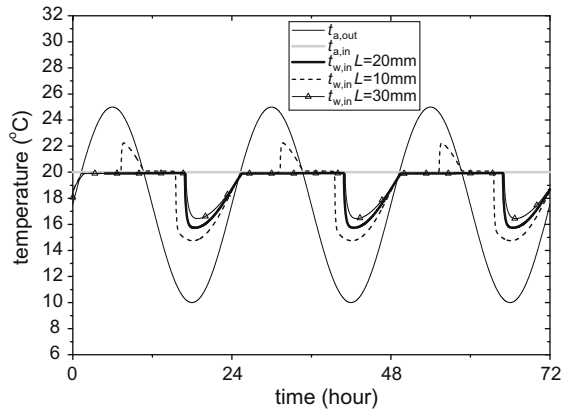

Fig. 9. Hourly inner surface temperature for various thickness of the SSPCM wallboard.

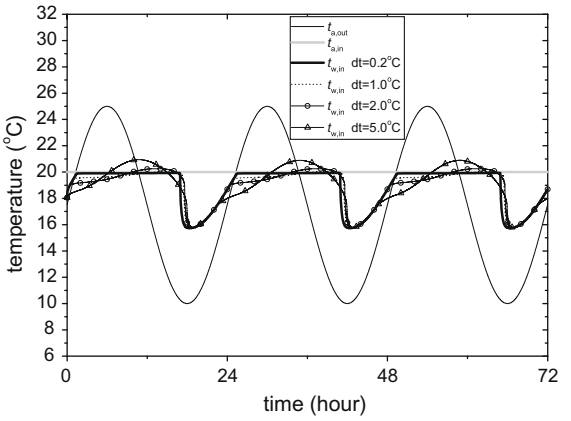

Fig. 10. Hourly inner surface temperature for various phase transition zone of the SSPCM.

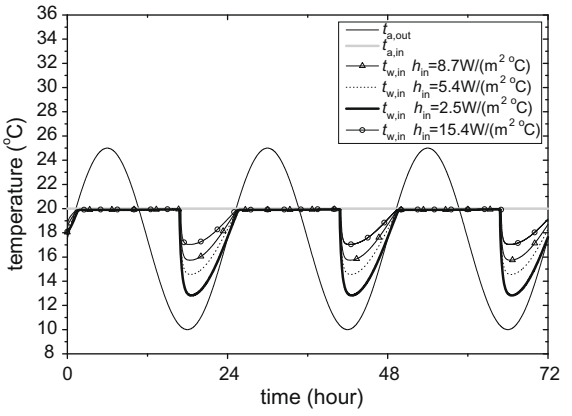

Fig. 11. Hourly inner surface temperature for various inner surface convective coefficients.

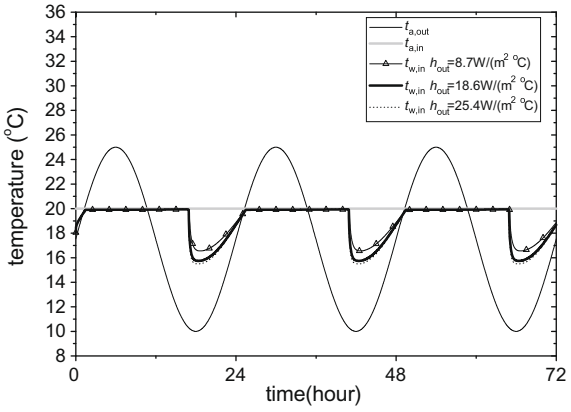

Fig. 12. Hourly inner surface temperature for various outer surface convective coefficients.

W m^{-2} °C^{-1} and h_{out} = 25.4 Wm^{-2} °C^{-1}, which correspond to the normal range of outdoor air velocity.

6. Conclusions

Thermal characteristics of shape-stabilized phase change material (SSPCM) wallboard with sinusoidal temperature wave on the outer surface were investigated numerically and compared with traditional building materials such as brick, foam concrete and expanded polystyrene (EPS). The calculated results showed that there exist flat segments within the inner surface temperature lines of SSPCM wallboard, which is distinct from the other three ordinary building materials, and the wave amplitude is considerably decreased due to the latent heat thermal storage. Phase transition keeping time of inner surface and decrement factor were applied to analyze the effects of PCM thermophysical properties (melting temperature, heat of fusion, phase transition zone and thermal conductivity), inner surface convective heat transfer coefficient and thickness of SSPCM wallboard. The results showed that melting temperature is one important factor which influences both the phase transition keeping time and the decrement factor; for a certain temperature wave, there exist critical values of latent heat of fusion and thickness of SSPCM above which the phase transition keeping time or the decrement factor are scarcely influenced; thermal conductivity of SSPCM and inner surface convective coefficient almost have no effects on the phase transition keeping time but significantly influence the decrement factor; outer surface convective coefficient slightly affects the decrement factor within the normal range of outdoor air velocity; and phase transition zone leads to small fluctuations of the original flat segment of inner surface temperature line. The results aim to be useful for the selection of SSPCMs and their applications in passive solar buildings and related areas.

Acknowledgements

This work was supported by the National Scientific and Technical supporting Program in the 11th "five-year" of China (No. 2006BAA04B02), Natural Science Foundation of Hebei Province (No. E2008001231) as well as the Doctoral Teacher Research Fund of North China Electric Power University (No. 200722012).

References

[1] Zhang YP, Lin KP, Zhang QL, Di HF. Ideal thermophysical properties for free-cooling (or heating) buildings with constant thermal physical property material. Energy Build 2006;38(10):1164–70.
[2] Zhang YP, Zhou GB, Lin KP, Zhang QL, Di HF. Application of latent heat thermal energy storage in buildings: state-of-the-art and outlook. Build Environ 2007;42(6):2197–209.
[3] Asan H, Sancaktar YS. Effects of wall's thermophysical properties on time lag and decrement factor. Energy Build 1998;28(2):159–66.
[4] Ulgen K. Experimental and theoretical investigation of effects of wall's thermophysical properties on time lag and decrement factor. Energy Build 2002;34(3):273–8.
[5] Peippo K, Kauranen P, Lund PD. Multicomponent PCM wall optimized for passive solar heating. Energy Build 1991;17(4):259–70.
[6] Athienitis AK, Liu C, Hawes D, Banu D, Feldman D. Investigation of the thermal performance of a passive solar test-room with wall latent heat storage. Build Environ 1997;32(5):405–10.
[7] Neeper DA. Thermal dynamics of wallboard with latent heat storage. Sol Energy 2000;68(5):393–403.
[8] Heim D, Clarke JA. Numerical modelling and thermal simulation of PCM-gypsum composites with ESP-r. Energy Build 2004;36(8):795–805.
[9] Inaba H, Tu P. Evaluation of thermophysical characteristics on shape-stabilized paraffin as a solid–liquid phase change material. Heat Mass Transfer 1997;32(4):307–12.
[10] Xiao M, Feng B, Gong KC. Preparation and performance of shape stabilized phase change thermal storage materials with high thermal conductivity. Energy Convers Manage 2002;43(1):103–8.
[11] Zhang YP, Yang R, Lin KP, Di HF, Jiang Y. Preparation, thermal performance and application of shape-stabilized PCM in energy efficient buildings. Energy Build 2006;38(10):1262–9.
[12] Ye H, Ge XS. Preparation of polyethylene–paraffin compound as a form-stable solid–liquid phase change material. Sol Energy Mater Sol Cells 2000;64(1):37–44.
[13] Zhang YP, Lin KP, Jiang Y, Zhou GB. Thermal storage and nonlinear heat transfer characteristics of PCM wallboard. Energy Build 2008;40(9):1771–9.
[14] Lin KP. Study of the application principles and effects for PCM building envelope components. Ph.D. Dissertation, Tsinghua University, Beijing; 2006.
[15] Li Z, Zhang YP, Jiang Y. Effect of specific heat of phase change material on heat charging or discharging performance. Acta Energiae Solaris Sinica 2002;23(1):27–31 [in Chinese].
[16] Tao WQ. Numerical heat transfer. 2nd ed. Xían: Xían Jiaotong University Press; 2001 [chapter 4, in Chinese].
[17] Solomon AD. An easily computable solution to a two-phase Stefan problem. Sol Energy 1979;23(6):525–8.
[18] Threlkeld JL. Thermal environmental engineering. NJ: Prentice-Hall; 1970.
[19] Asan H. Numerical computation of time lags and decrement factors for different building materials. Build Environ 2006;41(5):615–20.
[20] Wang WL, Yang XX, Fang YT, Ding J, Yan J. Enhanced thermal conductivity and thermal performance of form-stable composite phase change materials by using β-Aluminum nitride. Appl Energy 2009;86(7–8):1196–200.
[21] Wang WL, Yang XX, Fang YT, Ding J, Yan J. Preparation and thermal properties of polyethylene glycol/expanded graphite blends for energy storage. Appl Energy 2009;86(9):1479–83.
[22] ASHRAE. ASHRAE handbook – fundamentals. Heat transfer. Atlanta: ASHRAE; 2001 [chapter 3].
[23] Liu H, Awbi HB. Performance of phase change material boards under natural convection. Build Environ 2009;44(9):1788–93.
[24] Kuznik F, Virgone J. Experimental assessment of a phase change material for wall building use. Appl Energy 2009;86(10):2038–46.